Multipole electron densities and structural parameters from synchrotron powder X-ray diffraction data obtained with a MYTHEN detector system (OHGI)

Bjarke Svane,[a] Kasper Tolborg,[a] Kenichi Kato[b,c]* and Bo Brummerstedt Iversen[a]*

[a]Department of Chemistry, Aarhus University, Aarhus, DK-8000, Denmark, [b]RIKEN SPring-8 Center, 1-1-1 Kouto, Sayo-cho, Sayo-gun, Hyogo 679-5148, Japan, and [c]JST, PRESTO, 4-1-8 Honcho, Kawaguchi, Saitama 332-0012, Japan. *Correspondence e-mail: katok@spring8.or.jp, bo@chem.au.dk

Powder X-ray diffraction has some inherent advantages over traditional single-crystal X-ray diffraction in accurately determining electron densities and structural parameters due to the lower requirements for sample crystallinity, simpler corrections and measurement simultaneity. For some simple inorganic materials, it has been shown that these advantages can compensate for disadvantages such as peak overlap and error-prone background subtraction. Although it is challenging to extend powder X-ray diffraction-based electron-density studies to organic materials with significant peak overlap, previous results using a dedicated vacuum diffractometer with a large image-plate camera (AVID) demonstrated that it can be done. However, the vacuum setup with the off-line detector system was found to prohibit a widespread use. Fast microstrip detectors, which have been employed at a number of powder diffraction beamlines, have the potential to facilitate electron-density studies. Nevertheless, no electron-density studies even for materials with slight peak overlap have been performed with microstrip detectors. One of the most critical problems has been a difference in sensitivity between microstrip channels, which substantially defines the dynamic range of a detector. Recently, a robust approach to this problem has been developed and applied to a total scattering measurement system (OHGI) with 15 MYTHEN microstrip modules. In the present study, synchrotron powder X-ray diffraction data obtained with OHGI are evaulated in terms of multipole electron densities and structural parameters (atomic positions and displacement parameters). These results show that, even without a dedicated setup and perfect samples, electron-density modelling can be carried out on high-quality powder X-ray diffraction data. However, it was also found that the required prior information about the sample prohibits widespread use of the method. With the presently obtainable data quality, electron densities of molecular crystals in general are not reliably obtained from powder data, but it is an excellent, possibly superior, alternative to single-crystal measurements for small-unit-cell inorganic solids. If aspherical atomic scattering factors can be obtained from other means (multipole databases, theoretical calculations), then atomic positions (including for hydrogen) and anisotropic atomic displacement parameters (non-hydrogen atoms) of excellent accuracy can be refined from synchrotron powder X-ray diffraction data on organic crystals.
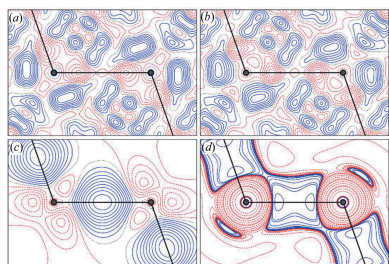
1. Introduction

Virtually all experimental electron densities (EDs) are determined from structure factors extracted from single-crystal X-ray diffraction (SCXRD), since this has been regarded as the optimal way to obtain data of the highest quality (Koritsanszky & Coppens, 2001; Jørgensen *et al.*, 2014). Accurate determination of the ED places significantly higher requirements on the quality of the measured data than

conventional crystal structure determination in terms of accuracy, redundancy and resolution. This is because an increased number of parameters needs to be refined, and EDs are closely correlated with atomic displacement parameters (ADPs) (Figgis *et al.*, 1993; Bindzus *et al.*, 2014). In addition, corrections for sample absorption, extinction effects and scale-factor fluctuations must be properly applied to obtain reliable EDs (Iversen *et al.*, 1996). Improper corrections for these effects give rise to systematic errors in structure factors, which reduce the quality of the obtained ED distribution.

For the relatively light atoms predominant in organic compounds, accurate ADP determination depends on an appropriate description of the atomic ED if it is significantly aspherical. Reliable EDs of many small molecules can be readily obtained on the basis of theory, while the theoretical determination of ADPs is not yet well established (Madsen *et al.*, 2013). If aspherical atomic scattering factors for the bonded atoms in molecular crystals are known from external sources such as multipole databases like ELMAM (Zarychta *et al.*, 2007; Domagała *et al.*, 2012; Nassour *et al.*, 2017), INVARIOM (Dittrich *et al.*, 2004; 2013) or UBDB (Volkov *et al.*, 2004; Kumar *et al.*, 2019), or by theoretical calculations as in the Hirshfeld atom refinement approach (Jayatilaka & Dittrich, 2008; Fugel *et al.*, 2018), then the accuracy of structural parameters (atomic positions and ADPs) can be significantly improved in refinement of SCXRD data. Such approaches have not been applied in refinement of powder X-ray diffraction data, but as shown below external aspherical atomic scattering factors can also greatly enhance the accuracy of structural information obtained from PXRD.

It has previously been shown that EDs can be successfully modelled in the Hansen–Coppens (HC) (Hansen & Coppens, 1978; Coppens, 1997) multipole formalism based on powder X-ray diffraction (PXRD) data instead of single-crystal (SC) data (Nishibori *et al.*, 2007; Svendsen *et al.*, 2010; Fischer *et al.*, 2011). A vacuum diffractometer with a large image-plate (IP) camera for synchrotron PXRD (SPXRD) ED studies, which is referred to as the Aarhus vacuum imaging-plate diffractometer (AVID) (Tolborg *et al.*, 2017; Straasø *et al.*, 2013), was developed to remedy drawbacks such as background-noise contamination and peak overlap. SPXRD data with low background noise yielded structure factors with high accuracy for single-element inorganic materials such as diamond (Bindzus *et al.*, 2014) and silicon (Tolborg *et al.*, 2017; Wahlberg *et al.*, 2016), in which case the significant extinction effect in SCXRD measurements makes it difficult to obtain accurate structure factors. Likewise, we have shown that EDs in qualitative agreement with SCXRD results can be obtained from simple molecular crystals such as urea, even though both crystal strain and significant peak overlap are present (Svane *et al.*, 2019). The latter study also showed that the AVID system (Tolborg *et al.*, 2017) had some significant drawbacks, *i.e.* a positional error introduced on IP digitization and a large point spread function. These issues severely limit the potential samples available for study, as an accurate peak position and width determination is critical to the quality of partitioning of overlapping reflections. A microstrip detector system using

MYTHEN (Bergamaschi *et al.*, 2010), which has a sharp line spread function and can be operated in real time, has the potential for increasing the productivity of reliable EDs for a variety of materials. However, MYTHEN systems have historically had problems with a lower-than-expected dynamic range, which causes issues for the reliable determination of intensities of both strong and weak reflections in a single exposure. The difference in X-ray response between channels, which is referred to as X-ray response non-uniformity (XRNU), has been recognized as one of the predominant factors to define the dynamic range of a detector system with a sharp line spread function. MYTHEN has a 24-bit counter for each channel, which corresponds to a dynamic range of 10^7. However, the dynamic range of a module was found to be 10^4 because of XRNU, which is lower than that of an IP detector. The flat-field parameters provided by the manufacturer failed in correcting XRNU. Recently, a data-driven approach, ReLiEf (response-to-light effector) (Kato *et al.*, 2019; Kato & Shigeta, 2020), was developed to restore the detector system to the original dynamic range. ReLiEf has been successfully applied to a total scattering measurement system, OHGI (overlapped high-grade intelligencer) (Kato *et al.*, 2019), which can cover a 2θ range from $3°$ to $156°$ with a step of $0.01°$ at the same time by placing 15 MYTHEN modules without a gap between modules. The camera radius (286.48 mm) is much smaller than that of AVID (1200 mm). The camera is not evacuated but a beam collimator and a beamstop at a distance of 30 mm from the sample reduce air scattering by incoming X-rays. At the same time, OHGI is more user-friendly and accessible.

Here, we assess the quality of structural parameters and ED modelling based on data collected on the high-resolution OHGI setup of the BL44B2 beamline at SPring-8 (Kato & Tanaka, 2016; Kato *et al.*, 2010, 2019; Kato & Shigeta, 2020) on diamond and the organic molecular crystals of urea and xylitol.

2. Experimental details

Crystalline diamond powder was purchased from Nilaco and packed in a 0.3 mm glass capillary. Urea crystals were purchased from Sigma–Aldrich as ACS reagent, 99.5%, CAS number 57-13-6. Xylitol was likewise purchased from Sigma–Aldrich, analytical standard, CAS number 87-99-0. Urea and xylitol crystals were ground carefully, sieved (20 μm mesh) and packed in a 0.2 mm glass capillary.

SPXRD data were collected using OHGI (Kato *et al.*, 2019) installed at the RIKEN Materials Science beamline BL44B2 (Kato & Tanaka, 2016; Kato *et al.*, 2010), SPring-8, Japan. The wavelength λ of the incoming X-rays was calibrated to be 0.45015 (1) Å by Le Bail refinement of a LaB_6 NIST standard reference material (SRM660b). The energy threshold of OHGI was set at 13.8 keV, which was half of the X-ray energy. Correction parameters for XRNU were collected using ReLiEf using the same setup. For the data treatment, incoming X-rays were considered to be totally polarized in a horizontal plane. The dimensions of incoming X-rays were

3 mm in horizontal length and 0.5 mm in vertical length. Data were collected up to 155.7° in 2θ (2.17 Å^{-1} in $\sin\theta/\lambda$) with a step of 0.005°, which was generated from two data sets obtained by shifting OHGI by 0.005°. The fine-step measurement did not improve the angular resolution, whereas the increased number of data points is expected to improve the accuracy of structure factors. The collection times for diamond, urea and xylitol were set to be 16 min, 15 min and 50 min, respectively. In order to compare OHGI data with AVID data (Bindzus et al., 2014; Svane et al., 2019) and a single-crystal neutron diffraction experiment (Madsen et al., 2003), diamond, urea and xylitol data were measured at room temperature, 100 K and 122 K, respectively.

3. OHGI data for EDs on simple inorganic systems

Simple, high-symmetry inorganic materials often pose a serious challenge to SCXRD data collection due to the presence of significant amounts of extinction (Schmøkel et al., 2013). Furthermore, such materials only possess relatively few diffraction peaks and therefore peak overlap is not present to a large degree. Thus, the ED has been obtained from SPXRD in multiple cases in the literature for simple systems such as diamond (Bindzus et al., 2014), silicon (Wahlberg et al., 2016) and boron nitride (Wahlberg et al., 2015). This makes these materials ideal for testing the performance of a new detector type and experimental setup for SPXRD, since it must offer adequate accuracy to successfully obtain an ED in agreement with previous SPXRD investigations and theoretical calculations.

Here, we choose diamond [space group $Fd\bar{3}m$, $a =$ 3.567286 (4) Å] as a benchmark system for testing the accuracy of the detector. The most accurate and extensive experimental determination of the ED in diamond is that of
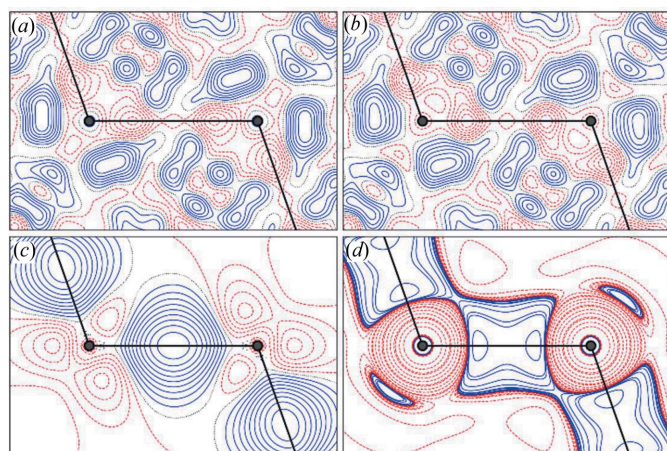
Figure 1
Density features in the (110) plane of diamond. (a) Residual density for the HC model, (b) residual density for the EHC model, (c) static model deformation density for the EHC model, and (d) negative Laplacian of the electron density for the EHC model. Positive, negative and zero contours are drawn in solid blue, dashed red and dotted black, respectively. Contour levels are drawn at 0.01 e Å^{-3} for (a) and (b), 0.05 e Å^{-3} (c), and at 0, $\pm1\times10^{n}$, $\pm2\times10^{n}$, $\pm4\times10^{n}$, $\pm8\times10^{n}$ e Å^{-5}, with $n = 0, \pm1, \pm2, \pm3$ (d).

Table 1
HC/Rietveld refinement parameters for OHGI data of diamond.

GOF is the Goodness of fit, whereas GU, GV, GW, LX and LY are Gaussian and Lorentzian peak shape parameters as implemented in *JANA2006* (Petříček et al., 2014).

	HC/Rietveld model	HC/Rietveld model with fixed U_{iso}
R/wR(obs) (%)	0.34/0.53	0.28/0.40
R_P/wR_P (%)	1.73/3.55	1.73/3.55
GOF	3.06	3.06
Scale	5.296 (8)	5.310 (5)
a (Å)	3.567286 (4)	3.567286 (4)
GU	1.7 (3)	1.6 (3)
GV	4.2 (1)	4.3 (1)
GW	0.77 (2)	0.76 (2)
LX	0.30 (1)	0.30 (1)
LY	2.81 (7)	2.78 (7)
Shift	0.153 (3)	0.152 (3)
U_{iso} (10^{-4} Å^2)	17.7 (2)	18.31 (16)†
κ_v	0.953 (4)	0.948 (3)
κ'_v	0.95 (1)	0.94 (1)
P_{32-}	0.307 (7)	0.308 (7)
P_{40}	−0.12 (1)	−0.12 (1)

† U_{iso} is fixed from the Wilson plot analysis. The uncertainty is determined from the weighted linear least-squares fit to the extracted structure factors.

Bindzus et al. (2014) using the original version of the AVID system (Straasø et al., 2013), which included experimental determination of the core electron deformation (Fischer et al., 2011). As they also thoroughly tested the methodology for obtaining the most accurate structure factors and ED, we employ the same methodology here. This consists of performing a combined HC/Rietveld refinement on the SPXRD data, in which the HC multipole parameters are included explicitly as free parameters in the Rietveld refinement. After convergence of the HC/Rietveld model, a Wilson plot analysis is performed using the extracted structure factors and static structure factors calculated using *Wien2k* to extract the ADP for carbon and a scale factor. This ADP is used iteratively as a fixed value in subsequent HC/Rietveld cycles until convergence, and the final model including core electron deformation is refined against the extracted structure factors with a fixed ADP and scale factor. For direct comparison with the results of Bindzus et al. (2014), we use the SCM scattering bank (Macchi & Coppens, 2001; Su & Coppens, 1998) with carbon in an sp^3 configuration, and a single-ζ density exponent of 3.156. For direct comparison, we only include data up to a resolution of $(\sin\theta/\lambda)_{max} = 1.7$ Å^{-1}. The results of the HC/Rietveld refinements are shown in Table 1 both for the model with a free U_{iso} and for the model with a fixed U_{iso} determined from a Wilson plot analysis.

A diagram showing the fit quality is shown in Fig. S1 in the supporting information. The results of the extended Hansen–Coppens (EHC) refinements on the extracted structure factors are shown in Table 2, and residual densities, deformation densities and Laplacians of the ED are shown in Fig. 1. First, we note the excellent agreement in terms of the refined parameters between OHGI data, AVID data and theory. Note that the thermal parameters of carbon are consistent within one standard deviation, although this has previously been

Table 2
Refined parameters from EHC multipole refinements of diamond compared with theoretical calculations and data from AVID (Bindzus *et al.*, 2014).

For the experimental data, refinement is performed against structure factors extracted using the direct HC/Rietveld refinement of the powder data and iterative use of Wilson plots to extract a fixed thermal parameter and scale factor.

	OHGI (this study)	AVID (Bindzus *et al.*, 2014)	Wien2k (Bindzus *et al.*, 2014)
R_F (%)	0.25	0.26	0.03
U_{iso} (10^{-4} Å^2)	18.31 (16)†	18.19†	-
ρ_{min}/ρ_{max} (e Å^{-3})	$-0.07/0.07$	$-0.06/0.09$	$-0.01/0.01$
κ_v	0.945 (6)	0.958 (6)	0.971
κ'_v	0.93 (2)	0.86 (2)	0.876
P_{32-}	0.31 (2)	0.36 (2)	0.338
P_{40}	-0.13 (2)	-0.17 (2)	-0.105
P_v	4.003 (3)	4.013 (4)	4.014
κ_c	1.002 (1)	1.006 (1)	1.006
P_c	1.997 (3)	1.987 (4)	1.986
ρ_{BCP} (e Å^{-3})	1.64	1.66	1.61
$\nabla^2\rho_{BCP}$ (e Å^{-5})	-13.76	-13.61	-11.41
λ_3 (e Å^{-5})	7.97	8.17	9.10

† The estimated standard deviation on U_{iso} is given from weighted least-squares fit to the Wilson plot. It is not reported by Bindzus *et al.* (2014) from their analysis.

shown to be highly model dependent and difficult to obtain (Svendsen *et al.*, 2010). It is furthermore in excellent agreement with the value of 0.00189–0.00190 Å^2 from lattice dynamical calculations (Stewart, 1973), which serves as an upper limit to the value that should be obtained from X-ray diffraction, since systematic errors from thermal diffuse scattering tend to reduce the value obtained in a diffraction experiment.

In Fig. 1, it is interestingly observed that no large residual density is present in the core region of carbon, although the thermal parameter and the scale factor are kept fixed as obtained from the Wilson plot analysis. This is also reflected in the refined core parameters, which are close to free atom values compared with previous observations from AVID data and from *Wien2k* calculations. The subtle difference between OHGI and AVID results likely reflects the true uncertainty on experimental determination of core electron deformation, and thus more data are required to unequivocally determine the exact amount of core electron deformation in diamond. Nevertheless, the parameters can be refined and easily converge to the obtained values. Therefore, we conclude that the data quality allows for including core electron deformation features in the model, although the present data suggest they are small. The high data quality is also reflected in the very low residual density values.

As shown in Fig. 1, the expected chemical bonding features in diamond are well reflected in the present data, and the topological parameters are in good agreement with the previous benchmark determination from AVID and theory as seen from Table 2.

Thus, we may conclude that it is possible to obtain data of similar quality to those from dedicated setups employing vacuum to reduce the background level and a slow IP detector

system with this relatively simple and fast setup with OHGI. This allows for detailed ED modelling in inorganic materials with high crystal symmetry, for which peak overlap is not a significant issue in SPXRD.

4. OHGI data for molecular systems

ED determination from powder is severely complicated by the presence of peak overlap, as the quality of structure-factor extraction then relies on the accuracy of the peak profile and background description. Earlier studies using the AVID system (Svane *et al.*, 2019) were challenged by a peak position variation introduced by the scanner used to read the IP detector system. While there is no such variation present in the OHGI data, the higher background and wider peak profile are a significant source of structure-factor uncertainty. To determine the relative importance of these effects and evaluate the quality of ED determination from a conventional SPXRD instrument, we here compare EDs of urea determined from the OHGI system with those determined from the AVID system at beamline P08, PETRA III [λ = 0.49584 (2) Å]. Note that the model and general approach are similar to results published earlier on the AVID system (Svane *et al.*, 2019). The reader is referred there for details on AVID data collection and treatment.

Urea is a simple and well studied molecular crystal with both neutron (Swaminathan *et al.*, 1984) and high-quality SC data (Birkedal *et al.*, 2004; Zavodnik *et al.*, 1999) available. Urea is, however, known to have significant anisotropic strain-induced peak broadening. After the urea ED comparison, we investigate the quality of ED determination on the organic molecular compound xylitol. Xylitol has a lower symmetry and more atoms than urea, but the simpler peak profile description might outweigh these disadvantages.

4.1. Urea

Direct comparison of the powder diffractograms of urea (Table 3) collected on AVID and OHGI is shown in Fig. 2. The data are scaled to have the same integrated intensity as the 110
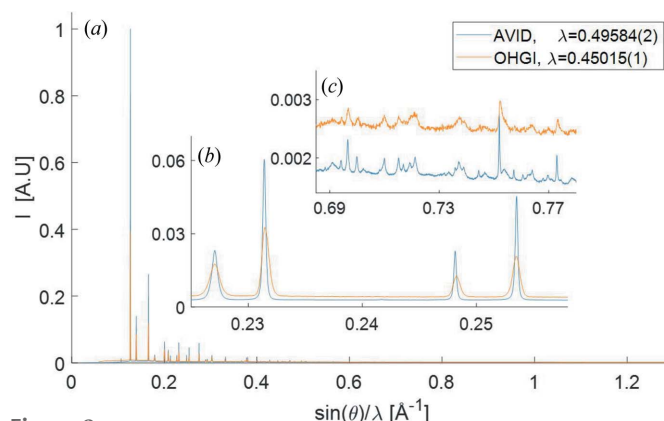
Figure 2
Integrated 1D SPXRD data on AVID and OHGI for urea. The data sets are scaled to have the same integrated intensity as the 110 reflection.
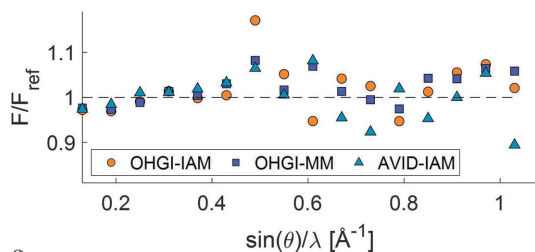
Figure 3
Temperature-corrected structure-factor amplitude relative to SC reference as a function of resolution for urea. Structure factors have been binned for readability. No weighting has been applied to reflections. The structure factors have been corrected for temperature difference as described in the text. The reference structure factors are from Birkedal *et al.* (2004). IAM refers to extraction using an independent atom model, while MM refers to extraction using a fixed aspherical atomic form factor from a SC refinement.

reflection. As expected, both the background and peak width are lower for AVID data, and more peaks are resolvable at high angles [Fig. 2(c)]. However, AVID uses an IP detector system known to have non-negligible positional errors, which give rise to systematic errors in the extracted structure factors (Tolborg *et al.*, 2017).

While the OHGI data extend to more than 150°, the lower signal-to-noise ratio at high angles makes reliable structure factors increasingly difficult to obtain. In the study of organic molecular crystals here, the data were cut at $2\theta = 58°$, corresponding to $\sin(\theta)/\lambda \simeq 1.07$ Å^{-1}, which is comparable with 1.00 Å^{-1} in the AVID data. This gives plenty of high-order reflections, which are necessary for accurate ADP determination, but a lower background level and more narrow peaks,

Table 3
Urea chemical information [unit-cell parameters from Birkedal *et al.* (2004)].

Chemical formula	$CO(NH_2)_2$
Space group	$P\bar{4}2_1m$
a (Å)	5.5780 (6)
c (Å)	4.6860 (7)
Structural drawing	
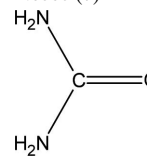
such as obtained from *e.g.* vacuum measurements or a larger sample-to-detector distance, would allow even higher-order reflections to be used, likely improving the ADP determination. In the present case using the full recorded data resolution decreased the quality of the subsequent refinement.

Structure factors are obtained from the 1D powder diffractograms using a Rietveld model in the program *JANA2006* (Petříček *et al.*, 2014). The methodology and refined parameters are included in the supporting information, Section S2. Structure-factor extraction was carried out with both spherical atomic form factors (IAM, independent atom model) and a simple HC (Hansen & Coppens, 1978) multipolar aspherical model. The multipole model included charge transfer between all atoms, all symmetry-allowed multipoles up to and including octupoles on C, O and N, and up to quadrupoles on H. A radial expansion/contraction parameter (κ) was refined for all non-hydrogen atoms and it was set to 1.16 for H atoms. The refinement used the Volkov–Macchi scattering bank based on relativistic density functional theory (DFT) calculations (Volkov & Macchi, unpublished work). This model is termed MM in the following section. MM corresponds to the model used in the multipolar refinement on extracted structure factors both in this and previous work (Svane *et al.*, 2019). Hydrogen-atom positions are determined from 123 K neutron data (Swaminathan *et al.*, 1984), while hydrogen ADPs are determined by scaling neutron values based on refined non-hydrogen ADPs using the program *UijXN* (Blessing, 1995).

To evaluate the quality of extracted structure factors, a direct comparison with reference SC values (Birkedal *et al.*, 2004) for both AVID and OHGI is shown in Fig. 3. The effect of a temperature difference with respect to the SC reference is corrected with a linear fit to the equation $\ln(F_{obs}^2/F_{ref}^2) = \ln(k) - 2B\sin^2(\theta)/\lambda^2$, calculating the corrected structure factors as $F_{obs,cor} =$
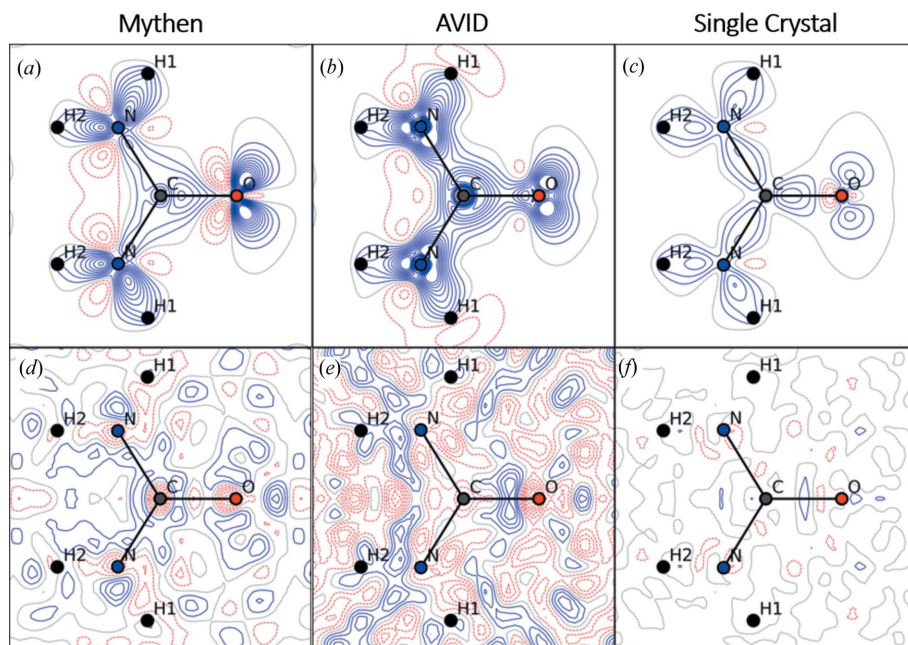

Figure 4
Static deformation density (*a*)–(*c*) and residual density (*d*)–(*f*) for models for urea based on extracted powder structure-factor lists compared with single crystal (Birkedal *et al.*, 2004). The OHGI structure-factor list is extracted using the aspherical atomic density (MM), which gave better results than the IAM extraction. The AVID plots are based on IAM-extracted structure factors. Contour levels are 0.2 and 0.05 e Å^{-3} for the deformation and residual density, respectively.

Table 4
Direct comparison of temperature-corrected OHGI and AVID extracted structure factors of urea with reference SC data of Birkedal *et al.* (2004).

$R(F) = \sum(|F - F_{ref}|)/\sum(F_{ref})$ is the reliability factor and $\langle F/F_{ref} \rangle$ is the average ratio.

	$R(F)$	$\langle F/F_{ref} \rangle$
OHGI–IAM	0.1043	1.0345
OHGI–MM	0.0680	1.0366
AVID–IAM	0.0715	0.9976

Table 5
ADP evaluation.

Neutron reference based on linear interpolation between neutron 123 K and 60 K data sets by Swaminathan *et al.* (1984). SC reference by Birkedal *et al.* (2004) is compared with unscaled neutron values.

	$\langle U_X^{ii}/U_N^{ii} \rangle$	$\langle |\Delta U_{X-N}^{ij}| \rangle$	$\langle |\Delta U_{X-N}^{ii}| \rangle$	wRMSD
OHGI–IAM	1.32 (7)	0.0045 (6)	0.0040 (7)	13.24
OHGI–MM	1.02 (5)	0.0017 (5)	0.0018 (6)	4.38
AVID–IAM	0.86 (7)	0.0014 (9)	0.0018 (9)	2.80
SC reference	1.03 (4)	0.0004 (4)	0.0003 (4)	1.59

$F_{obs} k \exp[B \sin^2(\theta)/\lambda^2]$, where k is a scaling constant and $B = 8\pi^2 \Delta U_{iso}$.

As shown in detail in a previous study (Svane *et al.*, 2019), the atomic density model only has a small impact on the quality of the resulting structure factors. While the AVID data surprisingly showed little difference between the ED models used for extraction, possibly even giving a slightly better overall fit for the IAM model, the OHGI data show a significant increase in fit quality, if structure factors are extracted with a simple multipolar model compared with IAM [decreasing $R(F)$ from 0.1043 to 0.0682; see Table 4]. For this reason, the two OHGI models will subsequently only be compared with AVID–IAM and not both AVID data models.

Structure factors extracted using IAM and MM are modelled identically by refining a model identical to MM. The extraction model thus only serves to correctly partition the intensity between overlapping reflections. To inspect the quality of ED modelling based on extracted structure factors, static model deformation densities and residual densities from both OHGI and AVID data are shown in Fig. 4. Refinement parameters for the multipolar models are given in Table S2.

ED concentrations in covalent bonds and oxygen lone pairs are captured by the powder-based data [Figs. 4(*a*), 4(*b*)]. Comparison between OHGI and AVID data shows that the residuals are significantly lower for the OHGI data set than for AVID. The deformation density around atomic cores has more reasonable levels for the OHGI data, but is still higher than for SC, which is possibly attributable to the radial inflexibility of the chosen HC model. High residuals in the OHGI data set are primarily located around heavy-atom nuclei [Fig. 4(*d*)]. The correlated residual signal suggests that the modelling on extraction is inadequate. The features can be explained by the higher background in the OHGI experiment, which complicates the accurate extraction of high-order peaks that are most affected by atomic displacements. A further indication that the OHGI data atomic positions and displacements are a primary source of residuals is the absence of large residuals around the H atoms, for which atomic positions and displacements are not refined. It is reasonable to expect that the residuals around the heavy atoms would be significantly reduced if the background intensity was reduced by *e.g.* performing the experiment in vacuum or using a larger sample-to-detector distance, as is the case for AVID data.

While the low-order peaks are well resolved using OHGI, giving a reasonable ED description, the high-order peaks are not appropriately deconvoluted. This is likely because of the lower signal-to-noise ratio compared with AVID data. It is reasonable to expect that this would negatively affect the obtainable ADPs. This is evaluated in Table 5 using the mean trace ratio, $\langle U_X^{ii}/U_N^{ii} \rangle$, the mean absolute difference of all ADPs, $\langle |\Delta U_{X-N}^{ij}| \rangle$, the mean absolute trace difference between X-ray and neutron ADPs, $\langle |\Delta U_{X-N}^{ii}| \rangle$, and

$$\text{wRMSD} = \left\{ \left\langle (U_X^{ij} - U_N^{ij})^2 / [\sigma(U_X^{ij})^2 + \sigma(U_N^{ij})^2] \right\rangle \right\}^{1/2}$$

which accounts for the combined errors in both experiments (Iversen *et al.*, 1996; Fugel *et al.*, 2018).

In general, the difference from neutron ADPs is approximately equal for the AVID and OHGI data. Multipolar structure-factor extraction is a significant improvement over IAM for OHGI data. This can be interpreted as the vibrational model absorbing part of the errors introduced by describing the atomic ED as spherical. The OHGI–MM refinement gives a mean trace ratio very close to unity, indicating good agreement between the OHGI and neutron ADPs. However, the relatively larger $\langle |\Delta U_{X-N}^{ii}| \rangle$ shows that this is caused by equal deviations above and below the neutron value. The higher wRMSD for the OHGI data can be explained by the deconvolution issues that were already apparent in the static deformation density plots [Figs. 4(*a*)–4(*c*)]. It is also likely affected by the lower estimates of uncertainty on OHGI data compared with the AVID data, where the uncertainty is increased through a scanner position error (Tolborg *et al.*, 2017). In general, AVID and OHGI data perform approximately equally well, but significantly worse than the single-crystal reference data.
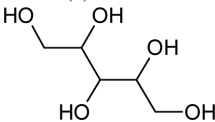
These results show that good ED descriptions are obtainable without evacuating and enlarging the powder camera from an excellent non-dedicated experimental setup with short measuring time, making powder EDs a more attractive alternative. The OHGI data presented here also indicate that it might be advantageous to deconvolute the ADPs and ED by determining the atomic positions and displacements through an alternative method. Apart from neutron measurements, the SHADE database for hydrogen atoms (Madsen, 2006) or a Hirshfeld atom refinement procedure for atomic EDs (Jayatilaka & Dittrich, 2008; Capelli *et al.*, 2014) could provide complementary information.

4.2. Xylitol

As mentioned previously, urea crystals are known to contain significant strain, which exacerbates any intensity

Table 6
Xylitol chemical information [unit-cell parameters from Madsen *et al.* (2004)].

Chemical formula	$C_5H_{12}O_5$
Space group	$P2_12_12_1$
a (Å)	8.2660 (4)
b (Å)	8.8977 (4)
c (Å)	8.9116 (4)
Structural drawing	

Table 7
Direct structure-factor comparison between extracted SPXRD (OHGI) and SCXRD (reference) for xylitol.

$R(F) = \sum(|F - F_{ref}|)/\sum(F_{ref})$ is the reliability factor and $\langle F/F_{ref}\rangle$ is the average ratio.

	$R(F)$	$\langle F/F_{ref}\rangle$
IAM	0.1732	1.0112
MM	0.1511	1.0510
MM–XYZU	0.0514	1.0402

partitioning issues. To assess the quality of ED determination from powder in the absence of this complication, high-quality SPXRD data on the relatively simple molecular compound xylitol have been collected using OHGI in the same experimental setup as described for urea. Xylitol (Table 6) has been thoroughly studied in the charge density community (Madsen *et al.*, 2004; Hoser & Madsen, 2017), including the collection of a high-quality neutron diffraction data set (Madsen *et al.*, 2003). However, it should be noted that xylitol crystallizes in a non-centrosymmetric space group, which inevitably results in a more challenging ED refinement due to the phase uncertainty. Thus, studying an ideal centrosymmetric organic molecular crystal may result in a better SPXRD ED determination than for xylitol.

The procedure for the xylitol data treatment is similar to that for urea. The Rietveld profile model used in structure-factor extraction is fairly simple and can be seen in the supporting information, Section S4. Three different models are compared in the rest of this section: IAM, where the atomic positions and vibrations of non-H atoms are refined, while H atoms are fixed at neutron values and the atomic form factors are spherical, MM which instead employs aspherical atomic densities obtained from fitting to SCXRD data published by Madsen *et al.* (2004), and finally MM–XYZU, where all atomic positions and vibrations are fixed at neutron values, and the scattering factor description is identical to that of MM. The MM aspherical description includes charge transfer between all atoms and all symmetry-allowed multipoles up to and including octupoles on C and O. For each H atom, all symmetry-allowed dipoles and quadrupoles are refined. A radial expansion/contraction parameter (κ) was refined for all non-hydrogen atoms and it was set to 1.16 for H atoms. The model uses the Volkov–Macchi scattering bank
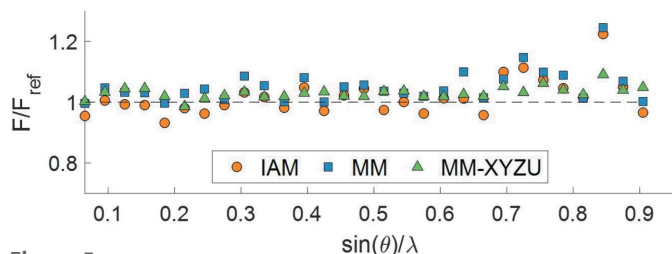

Figure 5
Binned relative structure-factor amplitude as a function of $\sin(\theta)/\lambda$ for xylitol. No weighting has been applied to reflections.

based on relativistic DFT calculations (Volkov & Macchi, unpublished work). Refinement of the profile against low-order peaks, where peak overlap is less significant, did not improve the extraction results.

The three extraction models give quite different results, as can be seen in Fig. 5, where structure-factor lists are compared with the SC reference data set. The agreement is quantified in Table 7. In general, the agreement is excellent at low angles but decreases at high angles. This is because the lower intensity and higher peak density make accurate extraction challenging. This trend is less pronounced for MM–XYZU, showing how a good determination of atomic positions and vibrations can impact the quality of the extracted structure factors. The impact of using aspherical atomic form factors is less than that of the positions and vibrations, but still results in a reduced residual factor.

The structure factors extracted from the different models are used to fit a flexible model with the same parameters as the MM extraction model. In the following, the models are termed based on the model used in structure-factor extraction, as the ED is modelled identically for all structure-factor lists.

Extracted structure factors are evaluated based on comparison of static deformation and residual density maps. Contour maps of planes intersecting three carbon atoms in the xylitol molecule are shown in Fig. 6. For clarity, the positions of atoms within 0.4 Å of the plane are also shown. Only the data extracted using the MM–XYZU model are shown here, with the rest of the maps being available in the supporting information, Section S5.

The SPXRD ED modelling qualitatively agrees with the SC experiment. Charge accumulation is observed in the covalent C—C bonds. Carbon sp^3 hybridization is distinctly visible. The ED around *e.g.* O1 and O2 shows a charge accumulation corresponding to the expected presence of an oxygen lone pair. The local charge depletion in C—O bonds, which is known to require a high data quality to resolve (Morgenroth *et al.*, 2008), is observed in multiple cases. In essence, all main features of the ED are captured by the SPXRD data, though the noise level is significantly higher. This is only the case, however, when the structure-factor extraction uses both an accurate aspherical atomic density, as well as fixed atomic positions and ADPs from the neutron data. The features observed in modelling of MM–XYZU structure factors are not resolvable if either of these requirements are not fulfilled, as is evident from inspection of Fig. S7. This is highly problematic for the application of SPXRD ED determination in general, as

Table 8
ADP evaluation for SPXRD (OHGI) data on xylitol.

The model names refer to the extraction models. Parameters are defined as in Section 4.1.

	$\langle U_X^{ii}/U_N^{ii}\rangle$	$\langle|\Delta U_{X-N}^{ij}|\rangle$	$\langle|\Delta U_{X-N}^{ij}|\rangle$	wRMSD
IAM	1.72 (9)	0.0071 (6)	0.0071 (6)	2.17
MM	1.53 (7)	0.0058 (5)	0.0058 (5)	1.70
MM–XYZU	1.14 (5)	0.0007 (5)	0.0007 (5)	2.14
SC reference	1.21 (6)	0.0012 (4)	0.0011 (4)	3.82

Table 9
Covalent bond lengths in urea.

OHGI–MM data are modelled with an ED locked to SC values, while all atomic positions and non-hydrogen-atom ADPs are refined freely. Hydrogen ADPs are kept fixed for Hpos, refined isotropically for Hiso and refined anisotropically for Hani. Neutron bond lengths are shown for comparison.

	OHGI–MM Hpos	OHGI–MM Hiso	OHGI–MM Hani	Neutron
C—O (Å)	1.250 (2)	1.249 (2)	1.250 (2)	1.257 (1)
C—N (Å)	1.337 (3)	1.337 (2)	1.338 (3)	1.339 (7)
N—H1 (Å)	0.986 (8)	0.981 (9)	0.974 (9)	1.005 (2)
N—H2 (Å)	1.009 (7)	1.008 (9)	1.038 (10)	0.996 (1)

some or all of these features are exactly what we usually conduct the experiment to determine. It is unreasonable to expect that a SPXRD experiment can bring more accurate and trustworthy information on a system, which already has a good ED description from e.g. a SC experiment and an accurate determination of atomic positions and ADPs such as from a neutron experiment.

The requirements on data and model quality for good EDs are high, and the current SPXRD methods do not allow a reasonable description in the absence of highly accurate positions and ADPs. In this regard, it is relevant to evaluate the degree of agreement between SPXRD and neutron refinements of these parameters. The evaluation results are shown in Table 8 using the same parameters as for urea. It is clear that if structure-factor extraction is carried out appropriately, as is the case for MM–XYZU, the agreement with neutron values is better than that of the SC data. Even using a slightly worse model in structure-factor extraction, the results are comparable, if slightly worse than the SC values. There is a notable effect of using aspherical atomic form factors in contrast to what was observed for urea. As the profile of xylitol peaks does not contain a significant strain contribution, it is less likely that the profile description will absorb the errors in the atomic form factors, which explains the observed

difference in ADP agreement that was not present in the urea study.

It should be stressed that the degree of peak overlap is significantly higher in xylitol than in urea, so the fact that a good deconvolution can be achieved gives confidence in SPXRD data as a source of accurate ADPs for small-molecule compounds if neutron data are not available. In any case, it should be emphasized that this conclusion is only reached when properly correcting the data for XRNU in the microstrip detectors.

4.3. Structural parameters from refinement with externally determined aspherical atomic scattering factors

To elucidate the effect of using externally determined aspherical atomic EDs to improve the quality of the structural parameters (atomic positions and ADPs), the OHGI MM extracted structure factors are modelled using an ED model locked to the SC description for both urea and xylitol. In essence, this corresponds to the ideal databank for transferable atom EDs.
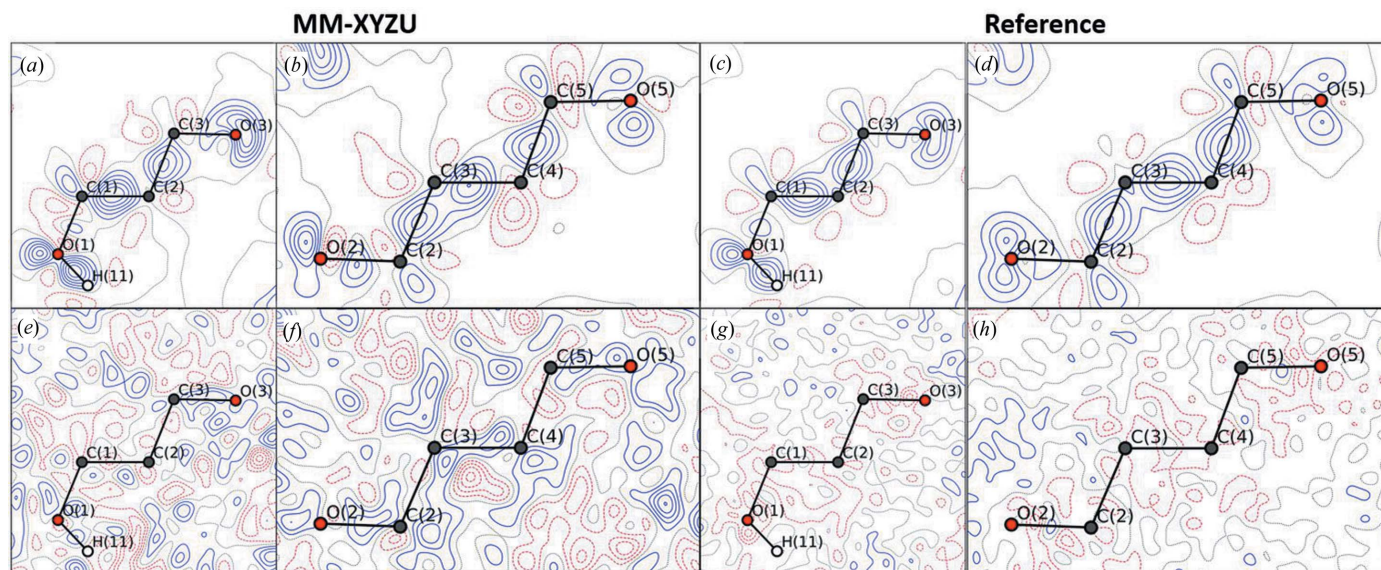
Figure 6
Contour plot of the plane intersecting C1, C2 and C3 and C3, C4 and C5 in xylitol. Static deformation density based on MM–XYZU extracted structure factors (a), (b) and reference SC structure factors by Madsen et al. (2004) (c), (d). Respective residual densities are shown below in (e), (f) and (g), (h). Contour levels are 0.1 e Å^{-3} and 0.05 e Å^{-3}, respectively. Positive and negative contour lines are shown in blue and red, respectively.

Table 10
ADP evaluation for non-hydrogen atoms and hydrogen atoms.

Neutron reference based on linear interpolation between neutron 123 K and 60 K data sets by Swaminathan *et al.* (1984).

	Non-H atoms				H atoms			
	$\langle U_X^{ii}/U_N^{ii}\rangle$	$\langle|\Delta U_{X-N}^{ii}|\rangle$	$\langle|\Delta U_{X-N}^{ii}|\rangle$	wRMSD	$\langle U_X^{ii}/U_N^{ii}\rangle$	$\langle|\Delta U_{X-N}^{ii}|\rangle$	$\langle|\Delta U_{X-N}^{ii}|\rangle$	wRMSD
OHGI–MM Hpos	1.01 (4)	0.0017 (5)	0.0017 (5)	4.63	1.27 (5)	0.0034 (8)	0.0054 (8)	5.49
OHGI–MM Hiso	1.02 (4)	0.0017 (5)	0.0017 (5)	4.65	2.2 (2)	0.016 (2)	0.018 (3)	8.94
OHGI–MM Hani	1.03 (5)	0.0017 (5)	0.0017 (5)	4.79	1.5 (3)	0.017 (5)	0.017 (5)	4.64

Table 11
Xylitol bond lengths for SPXRD (OHGI) refinements with externally determined aspherical atomic scattering factors as well as reference neutron values.

The model names refer to the extraction model. Bond lengths are given in units of Å. RMSD is the relative root-mean-square deviation from neutron bond lengths.

	IAM	MM	MM–XYZU	Neutron
C1—C2	1.5797 (3)	1.5523 (2)	1.51598 (4)	1.5151 (1)
C2—C3	1.4892 (3)	1.4938 (2)	1.5352 (1)	1.5332 (1)
C3—C4	1.5493 (3)	1.5395 (2)	1.52963 (9)	1.52931 (8)
C4—C5	1.4786 (5)	1.4922 (2)	1.51941(6)	1.5206 (2)
C1—O1	1.4664 (4)	1.4569 (2)	1.4244 (1)	1.4236 (3)
C2—O2	1.4391 (3)	1.4387 (2)	1.42667 (9)	1.4276 (5)
C3—O3	1.4654 (2)	1.4347 (1)	1.4237 (2)	1.4242 (5)
C4—O4	1.4585 (5)	1.4261 (2)	1.4312 (1)	1.4323 (4)
C5—O5	1.4524 (4)	1.4271 (2)	1.4201 (1)	1.4203 (4)
O1—H1	1.06 (4)	1.07 (3)	0.99 (2)	0.998 (3)
O2—H2	1.03 (3)	1.01 (3)	1.02 (2)	0.979 (3)
O3—H3	1.16 (3)	1.11 (3)	0.97 (2)	0.986 (3)
O4—H4	1.12 (3)	1.05 (3)	1.01 (2)	0.972 (3)
O5—H5	1.11 (4)	0.98 (3)	0.99 (2)	0.987 (3)
C1—H1*a*	1.11 (3)	1.12 (2)	1.09 (2)	1.111 (4)
C1—H1*b*	1.19 (3)	1.15 (2)	1.03 (2)	1.101 (4)
C2—H2	1.16 (3)	1.09 (2)	1.09 (1)	1.104 (3)
C3—H3	1.18 (2)	1.14 (2)	1.11 (1)	1.111 (3)
C4—H4	1.18 (3)	1.12 (2)	1.11 (2)	1.103 (3)
C5—H5*a*	1.18 (3)	1.07 (2)	1.07 (2)	1.099 (4)
C5—H5*b*	1.30 (3)	1.15 (2)	1.09 (2)	1.108 (4)
RMSD (non-H)	2.63%	1.62%	0.07%	-
RMSD (H)	10.40%	5.23%	2.78%	-

We first analyse the urea data and here the heavy-atom positions and ADPs were refined. To test both the data quality and the success of the deconvolution of the ED, hydrogen-atom positions were also refined. Hydrogen ADPs are either locked at the scaled neutron values, refined isotropically or refined anisotropically. All refinements converged without issues. The results are shown in Table 9 in terms of covalent bond lengths and in Table 10 in terms of ADPs for non-hydrogen atoms.

These results for the molecular geometry are extremely promising, and they indicate that with an externally determined ED, *e.g.* from multipole databases or Hirshfeld atom refinement, SPXRD data can provide very accurate bond lengths, even to the point of allowing the refinement of hydrogen-atom positions with an accuracy of a few per cent. The refined heavy-atom ADPs are on average 0.0017 Å^2 different from the neutron values for the non-hydrogen atoms, and thus the present study demonstrates that state-of-the-art SPXRD data can provide very meaningful anisotropic ADPs.

For the hydrogen atoms the ADPs are an order of magnitude less accurate, but the comparison with the neutron data is not much worse than the results obtained from Hirshfeld atom refinement of single-crystal data or use of databases such as SHADE (Fugel *et al.*, 2018). Clearly, accurate determination of hydrogen ADPs is best done with single-crystal neutron diffraction.

Xylitol is a larger molecule, which crystallizes in a non-centrosymmetric space group. Using the SC ED model as the external 'database' ED model, the atomic positions including hydrogen positions were refined on the three different extracted data sets. In addition, all non-hydrogen ADPs were refined, while hydrogen ADPs were fixed at anisotropic neutron values. The resulting bond lengths are shown in Table 11.

For xylitol, the agreement in bond lengths between SPXRD and neutron data is quite poor for the IAM and MM extraction models and in general inferior to refinement of SC data. A clear difference is observed when using the MM–XYZU structure-factor list, where atomic positions and ADPs were fixed to neutron values during extraction. Here, the agreement for both heavy-atom and hydrogen-atom positions is reasonably good. This suggests that if an iterative scheme is used, which is capable of progressively improving the extraction model, SPXRD could provide a valuable alternative to SC and neutron diffraction as a source of reliable structural parameters including hydrogen positions.

Isotropic and anisotropic ADP refinement on hydrogen atoms was attempted for xylitol, but rejected, since the resulting ADPs were in very poor agreement with neutron values.

5. Related literature

The following reference is cited in the supporting information: Stephens (1999).

6. Conclusion

To conclude, we have shown that it is possible to obtain an experimental ED from SPXRD data using the excellent but also user-accessible modern SPXRD setup OHGI, with a quality similar to that obtained from a dedicated setup performing diffraction in vacuum. For simple inorganic solids, here diamond, it is possible to obtain high-quality data even allowing for refinement of core electron deformation,

although the present data suggest the effect to be smaller than found in previous analyses. In the case of simple inorganic solids, SPXRD is a valuable alternative to SCXRD for ED modelling, since extinction and absorption effects, reducing the quality of SCXRD data, are removed, and peak overlap in the SPXRD is not a significant issue due to the small unit cell and high symmetry.

For molecular crystals the amount of peak overlap is significantly increased, and this significantly challenges the structure-factor extraction. For urea, a molecule with only five independent atoms crystallizing in a non-centrosymmetric space group, the SPXRD ED qualitatively agrees well with the SC reference ED. Furthermore, excellent structural parameters can be obtained, even for hydrogen atoms, and for the non-hydrogen atoms reliable anisotropic ADPs are retrieved.

In the case of xylitol, which is a larger molecule crystallizing in a non-centrosymmetric space group, a reasonable quality ED is only obtainable if structural parameters and aspherical atomic scattering factors are available from a different source and applied in the Rietveld refinement structure-factor extraction. This information can come from SCXRD experiments, multipole databanks or from theory. It is questionable if the SPXRD ED in this case adds additional information compared with the model used as input in the structure-factor extraction.

For many important systems, it is impossible to grow the high-quality single crystals needed for determination of accurate atomic positions and ADPs from SC experiments. In this case, an externally determined ED can be used to obtain highly accurate structural parameters from SPXRD data. Such external EDs can be obtained *e.g.* from multipole databanks or theoretical calculations, and the structural refinement is then comparable *e.g.* to the Hirshfeld atom refinement scheme. For urea, the structural parameters obtained with external aspherical scattering factors are of very high quality, showing excellent agreement between SPXRD and neutron data even for hydrogen bond lengths and non-hydrogen anisotropic ADPs. For the non-centric xylitol, the agreement in bond lengths between SPXRD and neutron data is less good, but still quite acceptable. It appears that if an iterative scheme can be developed, which is capable of progressively improving the structure-factor extraction model, then SPXRD even in this case could become a valuable alternative to SC and neutron diffraction as a source of reliable structural parameters including hydrogen positions.

Overall, with the presently obtainable data quality, EDs of molecular crystals are not reliably obtained from SPXRD, whereas it is an outstanding alternative to SCXRD for small-unit-cell inorganic solids. Future improvements may result in higher-quality data, which may push the boundary for which systems can be studied with SPXRD. One relatively straight-forward improvement of instrumentation would be to combine the merits of the present OHGI setup with the merits of AVID, *i.e.* to perform diffraction in vacuum and increase the sample-to-detector distance, while maintaining a large angular coverage using several MYTHEN modules. However, significant improvements in terms of reduced peak overlap are needed for SPXRD to become a generally useful alternative for ED determination in molecular crystals.

References

Bergamaschi, A., Cervellino, A., Dinapoli, R., Gozzo, F., Henrich, B., Johnson, I., Kraft, P., Mozzanica, A., Schmitt, B. & Shi, X. (2010). *J. Synchrotron Rad.* **17**, 653–668.

Bindzus, N., Straasø, T., Wahlberg, N., Becker, J., Bjerg, L., Lock, N., Dippel, A.-C. & Iversen, B. B. (2014). *Acta Cryst.* A**70**, 39–48.

Birkedal, H., Madsen, D., Mathiesen, R. H., Knudsen, K., Weber, H.-P., Pattison, P. & Schwarzenbach, D. (2004). *Acta Cryst.* A**60**, 371–381.

Blessing, R. H. (1995). *Acta Cryst.* B**51**, 816–823.

Capelli, S. C., Bürgi, H.-B., Dittrich, B., Grabowsky, S. & Jayatilaka, D. (2014). *IUCrJ*, **1**, 361–379.

Coppens, P. (1997). *X-ray Charge Densities and Chemical Bonding.* New York: Oxford University Press.

Dittrich, B., Hübschle, C. B., Pröpper, K., Dietrich, F., Stolper, T. & Holstein, J. J. (2013). *Acta Cryst.* B**69**, 91–104.

Dittrich, B., Koritsánszky, T. & Luger, P. (2004). *Angew. Chem. Int. Ed.* **43**, 2718–2721.

Domagała, S., Fournier, B., Liebschner, D., Guillot, B. & Jelsch, C. (2012). *Acta Cryst.* A**68**, 337–351.

Figgis, B. N., Iversen, B. B., Larson, F. K. & Reynolds, P. A. (1993). *Acta Cryst.* B**49**, 794–806.

Fischer, A., Tiana, D., Scherer, W., Batke, K., Eickerling, G., Svendsen, H., Bindzus, N. & Iversen, B. B. (2011). *J. Phys. Chem. A*, **115**, 13061–13071.

Fugel, M., Jayatilaka, D., Hupf, E., Overgaard, J., Hathwar, V. R., Macchi, P., Turner, M. J., Howard, J. A. K., Dolomanov, O. V., Puschmann, H., Iversen, B. B., Bürgi, H.-B. & Grabowsky, S. (2018). *IUCrJ*, **5**, 32–44.

Hansen, N. K. & Coppens, P. (1978). *Acta Cryst.* A**34**, 909–921.

Hoser, A. A. & Madsen, A. Ø. (2017). *Acta Cryst.* A**73**, 102–114.

Iversen, B. B., Larsen, F. K., Figgis, B. N., Reynolds, P. A. & Schultz, A. J. (1996). *Acta Cryst.* B**52**, 923–931.

Jayatilaka, D. & Dittrich, B. (2008). *Acta Cryst.* A**64**, 383–393.

Jørgensen, M. R. V., Hathwar, V. R., Bindzus, N., Wahlberg, N., Chen, Y.-S., Overgaard, J. & Iversen, B. B. (2014). *IUCrJ*, **1**, 267–280.

Kato, K., Hirose, R., Takemoto, M., Ha, S., Kim, J., Higuchi, M., Matsuda, R., Kitagawa, S., Takata, M., Garrett, R., Gentle, I., Nugent, K. & Wilkins, S. (2010). *AIP Conf. Proc.* **1234**, 875–878.

Kato, K. & Shigeta, K. (2020). *J. Synchrotron Rad.* **27**, 1172–1179.

Kato, K. & Tanaka, H. (2016). *Adv. Phys. X*, **1**, 55–80.

Kato, K., Tanaka, Y., Yamauchi, M., Ohara, K. & Hatsui, T. (2019). *J. Synchrotron Rad.* **26**, 762–773.

Koritsanszky, T. S. & Coppens, P. (2001). *Chem. Rev.* **101**, 1583–1628.

Kumar, P., Gruza, B., Bojarowski, S. A. & Dominiak, P. M. (2019). *Acta Cryst.* A**75**, 398–408.

Macchi, P. & Coppens, P. (2001). *Acta Cryst.* A**57**, 656–662.

Madsen, A. Ø. (2006). *J. Appl. Cryst.* **39**, 757–758.

Madsen, A. Ø., Mason, S. & Larsen, S. (2003). *Acta Cryst.* B**59**, 653–663.

Madsen, A. Ø., Sørensen, H. O., Flensburg, C., Stewart, R. F. & Larsen, S. (2004). *Acta Cryst.* A**60**, 550–561.

Madsen, A. Ø., Civalleri, B., Ferrabone, M., Pascale, F. & Erba, A. (2013). *Acta Cryst.* A**69**, 309–321.

Morgenroth, W., Overgaard, J., Clausen, H. F., Svendsen, H., Jørgensen, M. R. V., Larsen, F. K. & Iversen, B. B. (2008). *J. Appl. Cryst.* **41**, 846–853.

Nassour, A., Domagala, S., Guillot, B., Leduc, T., Lecomte, C. & Jelsch, C. (2017). *Acta Cryst.* B**73**, 610–625.

Nishibori, E., Sunaoshi, E., Yoshida, A., Aoyagi, S., Kato, K., Takata, M. & Sakata, M. (2007). *Acta Cryst.* A**63**, 43–52.

Petříček, V., Dušek, M. & Palatinus, L. (2014). *Z. Kristallogr.* **229**, 345–352.

Schmøkel, M. S., Bjerg, L., Larsen, F. K., Overgaard, J., Cenedese, S., Christensen, M., Madsen, G. K. H., Gatti, C., Nishibori, E., Sugimoto, K., Takata, M. & Iversen, B. B. (2013). *Acta Cryst.* A**69**, 570–582.

Stephens, P. W. (1999). *J. Appl. Cryst.* **32**, 281–289.

Stewart, R. F. (1973). *Acta Cryst.* A**29**, 602–605.

Straasø, T., Becker, J., Iversen, B. B. & Als-Nielsen, J. (2013). *J. Synchrotron Rad.* **20**, 98–104.

Su, Z. & Coppens, P. (1998). *Acta Cryst.* A**54**, 646–652.

Svane, B., Tolborg, K., Jørgensen, L. R., Roelsgaard, M., Jørgensen, M. R. V. & Brummerstedt Iversen, B. (2019). *Acta Cryst.* A**75**, 600–609.

Svendsen, H., Overgaard, J., Busselez, R., Arnaud, B., Rabiller, P., Kurita, A., Nishibori, E., Sakata, M., Takata, M. & Iversen, B. B. (2010). *Acta Cryst.* A**66**, 458–469.

Swaminathan, S., Craven, B. M. & McMullan, R. K. (1984). *Acta Cryst.* B**40**, 300–306.

Tolborg, K., Jørgensen, M. R. V., Christensen, S., Kasai, H., Becker, J., Walter, P., Dippel, A.-C., Als-Nielsen, J. & Iversen, B. B. (2017). *Acta Cryst.* B**73**, 521–530.

Volkov, A., Li, X., Koritsanszky, T. & Coppens, P. (2004). *J. Phys. Chem. A,* **108**, 4283–4300.

Wahlberg, N., Bindzus, N., Bjerg, L., Becker, J., Christensen, S., Dippel, A. C., Jørgensen, M. R. V. & Iversen, B. B. (2015). *J. Phys. Chem. C,* **119**, 6164–6173.

Wahlberg, N., Bindzus, N., Bjerg, L., Becker, J., Dippel, A.-C. & Iversen, B. B. (2016). *Acta Cryst.* A**72**, 28–35.

Zarychta, B., Pichon-Pesme, V., Guillot, B., Lecomte, C. & Jelsch, C. (2007). *Acta Cryst.* A**63**, 108–125.

Zavodnik, V., Stash, A., Tsirelson, V., de Vries, R. & Feil, D. (1999). *Acta Cryst.* B**55**, 45–54.